A Planar Electrooptic Beam Splitter with a Zig-Zag Electrode

CHUNG LEN LEE, MEMBER, IEEE, JING SHYANG HORNG, AND CHENG HAO HUANG

Abstract—**A new planar electrooptic beam splitter with a zig-zag electrode is proposed, studied, and demonstrated. The device is simple in its electrode configuration, hence, it is easier to be fabricated and has a potential to operate at higher speeds. Theoretical analyses on a single element of electrodes, as well as on the array structure, have been carried out, and experimental devices have been realized on $LiNbO_3$ to demonstrate its characteristics. The experimental results show that the device has a deflection power two times greater than that of a beam splitter with conventional electrodes. In addition, an analysis of the incident angle of the optical beam onto the device shows that the device can be used as a pure beam splitter, a beam deflector, or a combination of the two.**

I. INTRODUCTION

IN INTEGRATED OPTICS, various kinds of electrooptic and/or acoustooptic modulators [1]–[5], deflectors [6]–[8], and switches [9]–[13] have been invented, studied, and demonstrated. In 1975, Kaminow *et al.* [7] demonstrated a planar electrooptic switch which utilized an n-type electrode to simulate the prism structure to deflect an optical beam. This device is very simple in electrode configuration and can provide deflection into more than one position. The simulated prism n-type electrode can also be connected in parallel to form arrays in order to become a deflector [8]. In the array configuration, due to the constructive and destructive interference effects of neighboring units, an enhancement in the beam position resolution can be obtained. For this device, J. F. Revelli [14] had made a calculation and deduced that the maximum number of resolvable spots per centimeter of beamwidth could be on the order of 10^3, using a ± 500-V driving voltage and 50-μm prism aperture. A double-pole-double-throw switch also has been realized on a channel waveguide by C. L. Lee *et al.* [15]. There is a drawback for this simulated planar electrooptic electrode, however, which is that the phase shift created by the electrode, although linear at the central region, has a steeper variation near both edges of the aperture of the device. This nonlinear phase shift degrades the beam quality. To reduce this effect, a dogleg electrode configuration was proposed by Bulmer *et al.* [16], and it was studied in detail with two other modified electrode configurations by C. L. Lee *et al.*, [17] and an improvement in beam quality was obtained.

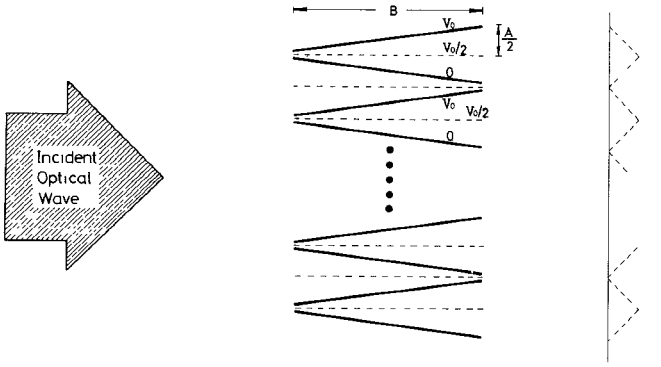

Fig. 1. The electrode configuration of a "zig-zag" electrooptic beam splitter. Virtual electrodes and the modulated wavefront on the optical wave are also shown.

In this paper, we propose and study a new type of electrode, a zig-zag electrode, which operates with a similar principle as the n-type prism electrode, while it also acts as a beam splitter. The electrode is shown in Fig. 1, where all the horizontal electrodes are eliminated and replaced by equivalent "virtual" electrodes. When a voltage V_0 is applied to electrodes as shown, the effective voltages on virtual electrodes are $V_0/2$. Due to the zig-zag configuration of electrodes, there are effectively two sets of prism arrays, with one array deflecting the optical beam into one direction and another array deflecting the optical beam into another direction. Hence, the device acts as a beam splitter. Because the electrode is simpler in configuration, it is easier to be fabricated and to operate at a higher speed (the electrode has a smaller capacitance) than the conventional n-type electrode prism array.

There is another advantage with this device, that is, in the conventional prism electrode array, due to the intrinsic photolithography limitation, there is a finite width required for electrodes and spacings between electrodes. This prevents the performance of the device from approaching the theoretical prediction in which zero width and spacings are assumed. Sidelobes are usually seen on the deflected and splitted beams. For the zig-zag electrode, all horizontal electrodes are eliminated. For each pair of tilt electrodes,

Manuscript received January 5, 1983; revised June 15, 1983. This work was sponsored by the National Science Council, Rep. of China under Contract NSC-71-0201-E009-10. Parts of the results of this paper had been presented at IEEE 1982 MTT-S Symposium on Microwaves, June, Dallas, TX.

C. L. Lee and J. S. Horng are with the Department of Electronic Engineering, National Chiao Tung University, Hsin Chu, Taiwan, Republic of China.

C. H. Huang is with the Chung Shan Institute of Science and Technology, Lung-Tai, Taiwan, Republic of China.

0018-9480/83/1100-0890$01.00 ©1983 IEEE

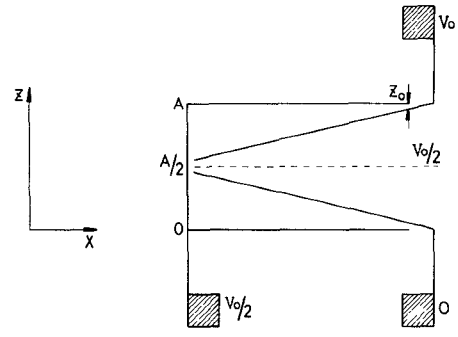

Fig. 2. A simulated single element of the zig-zag beam splitter.

one unit of the electrodes is reduced. The deflected or split beam then has a better quality.

In this paper, we first analyze the simulated "single" zig-zag electrode. Then an experimental device is fabricated and tested. The theoretical study indicates that the device not only behaves as a beam splitter, but also has a deflection angle two times greater than that of the conventional electrode of the same dimensions. Then the zig-zag array is studied. A physical device is also fabricated and tested. Finally, we analyze how the incident angle of the optical beam affects the device behavior. Using the concept of "virtual" electrodes, a general equation of the output deflection angle versus any incident angle θ is derived. If the incident angle is controlled properly, the device can operate either as an ideal beam splitter, deflector, or a combination of the two. An experimental demonstration concerning this result also is shown.

II. The Single Element of Zig-Zag Electrodes

In this section, a single element of the zig-zag electrode is analyzed first theoretically, and then studied experimentally. Fig. 2 is a single element of the zig-zag electrode. A "virtual" electrode is shown. In this figure, A and B are the aperture and length of the single element of electrodes, respectively, and Z and X are the crystal axes of $LiNbO_3$, on which the device is to be realized. To simulate the two "virtual" electrodes of the neighboring elements, real electrodes are placed and they are applied with a voltage of $V_0/2$ to imitate the effect of the two "virtual" electrodes.

With the voltages applied as shown in Fig. 2, the device can be, in effect, considered to be a combination of two conventional prism electrodes, with the "virtual" electrode being supplied with a voltage of $V_0/2$. Using

$$\eta(z) = (2\pi/\lambda)\int_0^B \Delta n\, dx \tag{1}$$

where η is the phase shift across the aperture of electrodes, λ is the wavelength of the light, and $\Delta n = n_e^3\gamma_{33}E_z/2$ is the index change induced by applied voltages, n_e and γ_{33} are the appropriate refractive index and $e-0$ constant of $LiNbO_3$ crystal, respectively, and E_z is the induced electric field between electrodes, the phase retardation $\eta(z)$, at the central regions ($z_0 < z < A/2 - z_0$ and $z_0 + A/2 < z < A - z_0$, where z_0 is the spacing between electrodes) can be derived to be

$$\eta(z) = \eta_0\left\{\left(\frac{z-z_0}{A/2-z}\right)^{1/2} - \left(\frac{A/2-z-z_0}{z}\right)^{1/2}\right\},$$
$$\text{for } z_0 < z < A/2 - z_0$$

or

$$= \eta_0\left\{\left(\frac{A-z_0-z}{z-A/2}\right)^{1/2} - \left(\frac{z-A/2-z_0}{A-z}\right)^{1/2}\right\},$$
$$\text{for } A/2 + z_0 < z < A - z_0 \tag{2}$$

where $\eta_0 = 2n_e^3\gamma_{33}V_0B/\lambda A$.

From (2), the normalization phase shift, $\eta(z)/\eta_0$, in terms of the normalized position in the aperture, i.e., z/A, is plotted in Fig. 3. It is found that a single element of zig-zag electrode induces two linear phase shifts with the same slope value but opposite signs. These two different phase retardations will cause the wavefront to be tilted into two symmetrical directions $\theta(z)$ as shown in the following expressions:

$$\theta(z) = \frac{\eta_0\lambda}{4\pi n_e}$$
$$\cdot\left\{\frac{A/2-z_0}{(A/2-z)^{3/2}(z-z_0)^{1/2}} + \frac{A/2-z_0}{z^{3/2}(A/2-z-z_0)^{1/2}}\right\},$$
$$\text{for } z_0 < z < A/2 - z_0$$

or

$$= \frac{-\eta_0\lambda}{4\pi n_e}\left\{\frac{A/2-z_0}{(z-A/2)^{3/2}(A-z-z_0)} + \frac{A/2-z_0}{(A-z)^{3/2}(z-A/2-z_0)^{1/2}}\right\},$$
$$\text{for } A/2 + z_0 < z < A - z_0. \tag{3}$$

The deflection angle in terms of the normalized aperture position is plotted in Fig. 4. From this figure, it is seen that the single zig-zag electrode behaves as a beam splitter. Its deflection angles are symmetrical with respect to the $V_0 = 0$ position and proportional to the applied voltage.

It should be mentioned that, in the expressions of $\eta(z)$ and $\theta(z)$, η_0 is the normalizing factor for the phase shift of the device. Comparing this factor with the one for a conventional prism deflector, it is found that it is two times greater since, in the expression for η_0, both the applied voltage and the aperture are half as large as those used in a conventional beam deflector. This will give this device two times greater deflection power than the conventional prism deflector.

An experimental device of Fig. 2 was fabricated on a Ti-diffused $LiNbO_3$ planar waveguide. The dimensions of the electrode were chosen to be $A = 110$ μm, $B = 3300$ μm, and $z_0 = 5$ μm, and the width of the electrode was 10 μm. The device was tested by coupling a 6328-Å optical wave into the electrode waveguide region. Fig. 5 is pictures of the output light spots taken at a distance 115 cm from the

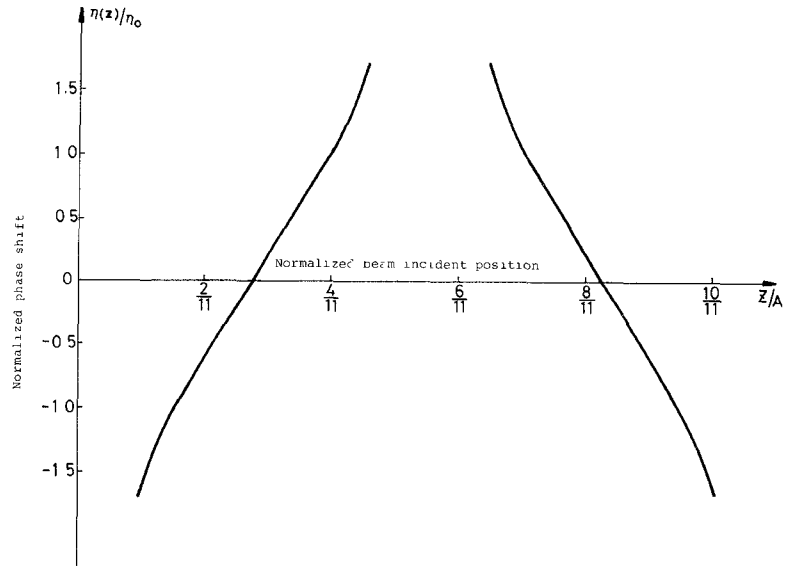

Fig. 3. The computed normalized phase shift on the passing optical wave versus the normalized incident position within the aperture A for the simulated single element zig-zag electrode.

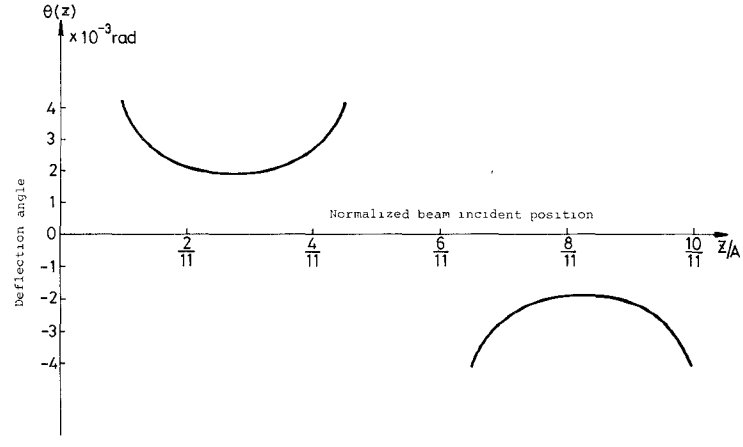

Fig. 4. The computed deflection angle of the optical wave versus the incident position for the simulated single-element zig-zag electrode.

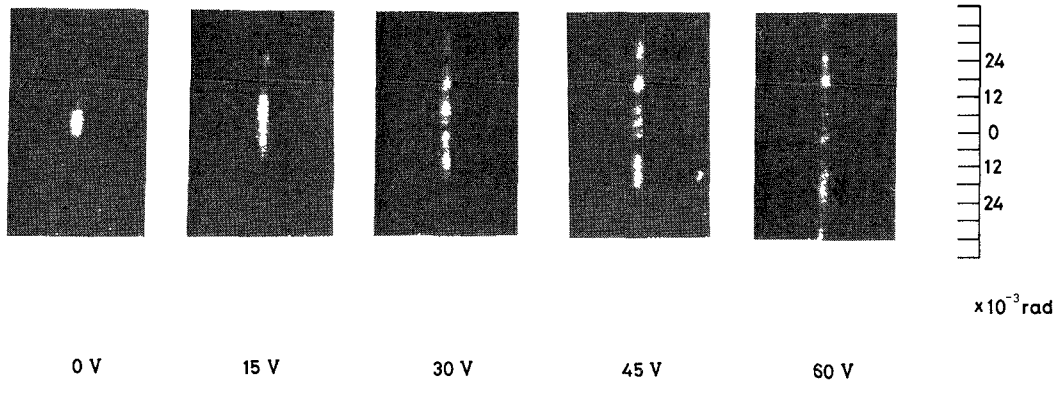

Fig. 5. The output beam spots of a realized single element zig-zag beam splitter under various applied voltages.

coupling-out prism with the applied voltage being 0, 15, 30, 45, and 60 V, respectively. In the figure, when the voltage is applied, the central light beam splits into two groups that are opposite in direction. For $V_0 = 30$ V, the central light spot is almost extinct, except for a small spot that is produced by the part of the light wave which does not pass through the electrode region. As the voltage is increased, these two groups of light spots continuously split further apart from the central position. This performance agrees with the theoretical prediction. However, the deflection angles obtained for this experimental device are 2.4 times greater than the theoretically calculated values. This phenomenon also occurs for the later case when the device is in an array structure. The reason for this discrepancy is unknown.

III. The Array Structure of Zig-Zag Electrodes

In this section, we will study the zig-zag electrode in an array structure. The electrode pattern is shown in Fig. 1. The device acts effectively as two sets of triangular phase gratings arranged alternatingly as shown.

For a phase grating structure, applying the Frannhofer–Kirchhoff diffraction formula [18], the diffraction intensity distribution can be obtained as follows:

$$I(p) = I_0 \frac{\sin^2(Kn_e pNA/2)}{\sin^2(Kn_e pA/2)} \left\{ \frac{\sin^2\left[\frac{KA}{4}(n_e p - 4\eta_0/KA)\right]}{K^2(n_e p - 4\eta_0/KA)^2} + \frac{\sin^2\left[\frac{KA}{4}(n_e p + 4\eta_0/KA)\right]}{K^2(n_e p + 4\eta_0/KA)^2} + \frac{2\cos\left(\frac{A}{2}Kn_e p + 2\eta_0\right)\cdot\sin\left[\frac{KA}{4}(n_e p - 4\eta_0/KA)\right]\cdot\sin\left[\frac{KA}{4}(n_e p + 4\eta_0/KA)\right]}{K^2\left(n_e^2 p^2 - 16\eta_0^2/K^2A^2\right)} \right\} \quad (4)$$

where N is the number of the period of the array, K is the wave number of the optical beam, $p = \sin\theta$, and θ is the angle between the observed direction and the normal direction of the phase grating.

In the above equation, the third term in the large parentheses is less than 1/15 of the first and second terms, so it is negligible. The term, $\sin^2(Kn_e pNA/2)/\sin^2(Kn_e pA/2)$, which is independent of the induced phase shift η_0, is the "array" factor. When $p = \sin\theta = \pm m(\lambda/n_e A)$, there are interference peaks for $m = 0, \pm 1, \pm 2, \cdots$. The terms in the large parentheses are the "intensity" factors, which represent a sinc function-type of intensity profile with two intensity peaks located at $p = \pm(\eta_0/(\pi/2))(\lambda/n_e A)$. The product of the "array" factor with the "intensity" factor, as voltage is applied, makes the central beam split into two groups of side beams with the beam of maximum intensity of each group located at $p = \pm(\eta_0/(\pi/2))(\lambda/n_e A)$. As the applied voltage is increased, these two groups of side beams split steadily further away. Figs. 6(a), (b), and (c) show the computed results, based on (4), on the intensity profiles for the applied voltage equal to 0, $V_{\pi/2}$ and $2V_{\pi/2}$, where $V_{\pi/2}$ is the applied voltage which induces a phase shift of $\eta_0 = \pi/2$. In the calculation, A was chosen to be 110 m, B was chosen to be 3300 μm, N was chosen to be 12, and $V_{\pi/2}$ was computed to be 26 V. In Fig. 6(b), $(V_0 = V_{\pi/2})$, the two groups of split side beams, overlap each other, with the peak intensity of each group located at $p/(\lambda/n_e A) = \pm 1$. In Fig. 6(c), $(V_0 = 2V_{\pi/2})$ has the two groups of side beams split completely, with the peak intensity of each group located at $p/(\lambda/n_e A) = \pm 2$. It can be seen that for a general case where $V_0 \neq mV_{\pi/2}$, the peak intensity for each side beam will fall into locations of $p/(\lambda/n_e A) \neq \pm m$.

An experimental device of the array structure also was fabricated and tested. The device was realized also on a Ti-diffused Y-cut X-propagation $LiNbO_3$ waveguide. The waveguide is a multiple-mode waveguide, but one with a fixed mode was chosen throughout our experiment. For the electrode, A, B, and N were chosen to be 110 μm, 3300 μm, and 12 μm, respectively. The width of the electrode and the spacings between electrodes were chosen to be 10 μm. A 6328-Å laser beam was coupled into the device. Fig. 7 shows the output spots of the device with the applied voltage to be 0, 15, 30, 45, and 60 V, respectively. With an applied voltage of 15 V, two split beams appear, with the central beam still observable. With the applied voltage increased to 30 V, the beam splits into two groups of side spots, with 3 spots for each group, and the central beam disappears completely. As the applied voltage is increased further, two groups of side spots split further away. These results agree with those of theoretical prediction. The deflection angles for each applied voltage, as mentioned in the single element device, are 2.4 times greater than the theoretically calculated values. However, this experimental device did demonstrate beam-splitter characteristics. Besides, it is noted that the light spots obtained with the array structure in Fig. 7 are much more well-defined than those obtained with the single element device of Fig. 5.

IV. Incident Angle Analysis

In Fig. 1, if the incident direction of the optical beam is not normal to the direction of the array, the device will not behave as a pure beam splitter. This can be seen by the following example: if the incident direction of the beam is in the direction of the electrode, i.e., the optical beam makes an angle of θ_d with the array as shown in Fig. 8(a), then the array will behave as a beam deflector. Hence, for an arbitrary optical beam, which makes an incident angle θ with respect to the array, the array will act partly as a

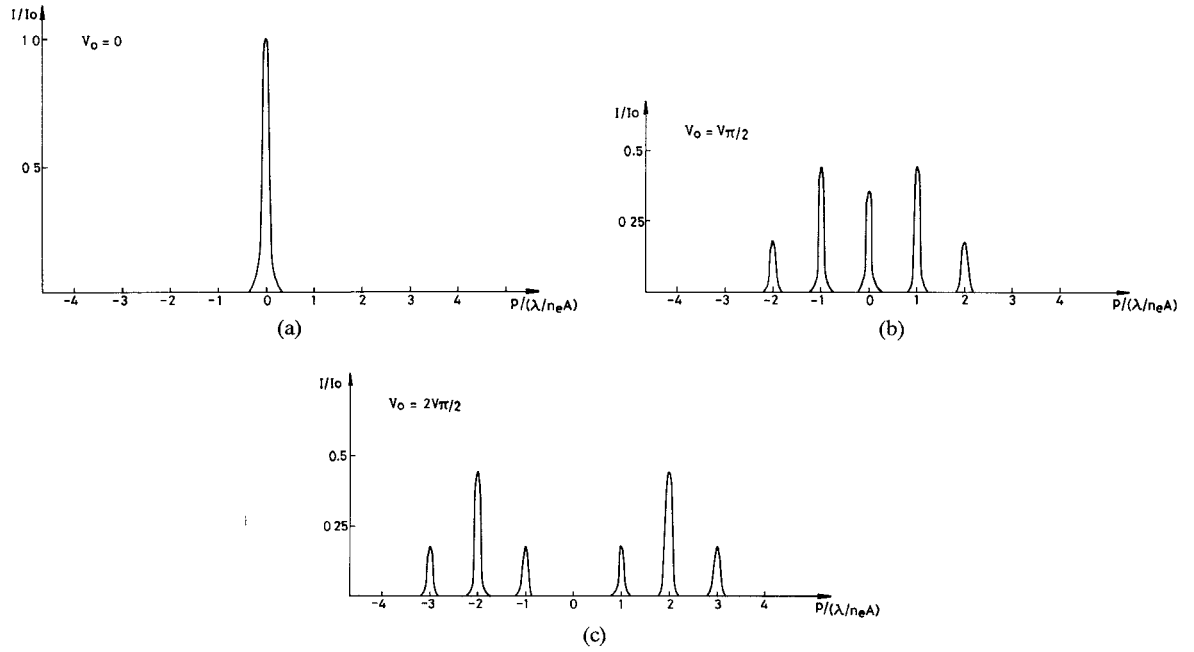

Fig. 6. The theoretically computed diffraction patterns of the zig-zag beam splitter for the applied voltage of (a) 0, (b) $V_{\pi/2}$, and (c) $2V_{\pi/2}$, where $V_{\pi/2}$ is the applied voltage which induces a phase shift of $\eta_0 = \pi/2$.

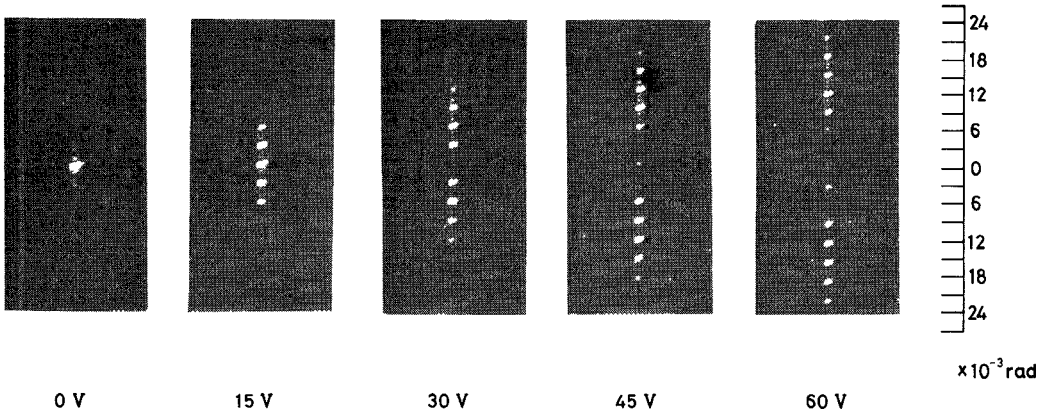

Fig. 7. The output beam spots for an experimental zig-zag array beam splitter under various applied voltages.

beam splitter and partly as a beam deflector. In this section, we study how the splitting (deflection) behavior of the device is affected by the incident angle of the optical beam.

We consider a general case as shown in Fig. 8(b). When the incident optical beam makes an angle θ with respect to the $V_0/2$ virtual axis, the electrode pattern can be equivalently viewed as that in Fig. 8(c). The electrode pattern is comprised of two sets of simulated prism elements with different apertures. The voltage on the virtual electrodes is

$$V = V_0(A/2 + B\sin\theta)/A. \tag{5}$$

Each set of simulated prism elements forms a deflector which deflects the beam into a different direction. The phase shift for each set of simulated prism deflectors also is shown in Fig. 8(c). If the same approximation proposed by Kaminow [7] is used, the deflection angle $\theta(z)$ can be obtained as

$$\theta(z) = \frac{n_e^2 \gamma_{33} V_0 (A/2 + B\sin\theta)}{2\pi bA} \cdot \left\{ \frac{A/2 + B\sin\theta - z_0}{(A/2 + B\sin\theta - z)^{3/2}(z - z_0)^{1/2}} + \frac{A/2 + B\sin\theta - z_0}{z^{3/2}(A/2 + B\sin\theta - z - z_0)^{1/2}} \right\},$$

$$\text{for } z_0 < z < A/2 + B\sin\theta - z_0$$

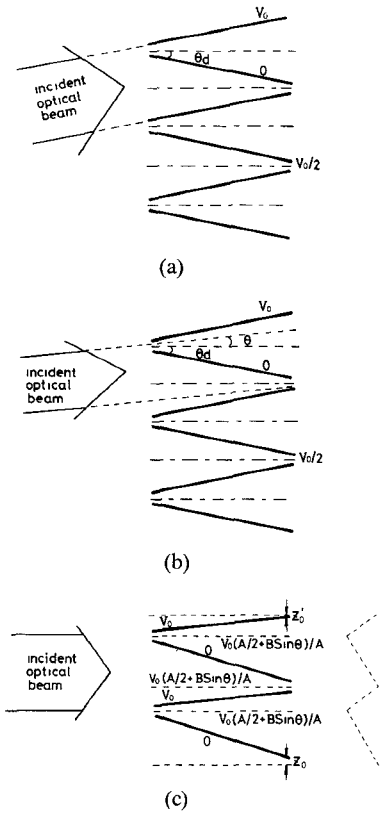

Fig. 8. (a) When the optical beam incidents at an angle θ_d, onto the device, where θ_d is the tilt angle of electrodes, the device is a beam deflector. (b) A general case that the optical beam incidents onto the device at an angle θ with respect to the array. (c) The incident optical beam equivalently sees two sets of prism arrays with different apertures.

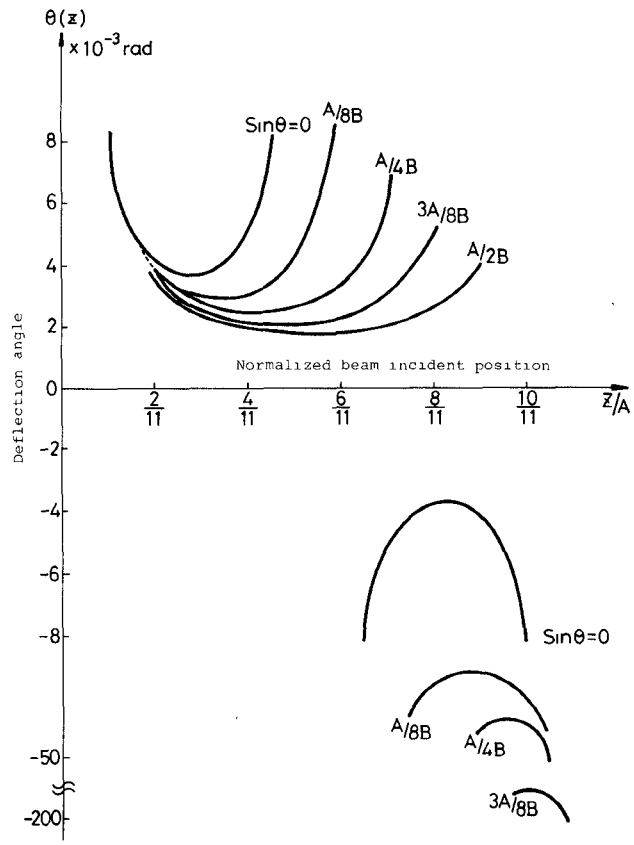

Fig. 9. The computed deflection angle of the incident optical beam versus the normalized incident position within the aperture A under various incident angles.

or

$$= \frac{-n_e^2\gamma_{33}V_0(A/2-B\sin\theta)}{2\pi b'A} \cdot \left\{ \frac{A/2+B\sin\theta-z_0'}{(z-A/2-B\sin\theta)^{3/2}(A-z-z_0')^{1/2}} + \frac{A/2+B\sin\theta-z_0'}{(A-z)^{3/2}(z-A/2-B\sin\theta-z_0')^{1/2}} \right\},$$

$$\text{for } A/2+B\sin\theta+z_0' < z < A-z_0' \quad (6)$$

where $b=(A/2+B\sin\theta-2z_0)/B$, $b'=(A/2-B\sin\theta-2z_0')/B$, and $z_0+z_0'=10$ μm, (z_0 and z_0' are functions of θ).

Equation (6) is a general equation which describes the deflection angle as a function of the incident angle. The deflection angles for $\sin\theta=0$, $A/8B$, $A/4B$, $3A/8B$, and $A/2B$, are plotted in Fig. 9. It is seen that the device behaves as an ideal beam splitter for $\sin\theta=0$. When θ is not zero, the device becomes a combination of a beam splitter and a beam deflector. As θ increases from zero, the intensity of the output light spot increases on one side, while the intensity of the light spot for the other side decreases (the envelopes of the deflected light beams represent the energies of deflected beams). It is also noticed that for the light spot of increased light intensity, the deflection angle becomes smaller, and for the light spot of decreased light intensity, the deflection angle becomes larger. For $\theta=\theta_d$, the intensity for one light spot will reach maximum and that for the other light spot will be zero. For this case, the device behaves as a pure deflector. If we decrease the incident angle from 0 to $-\theta_d$, similar results will be obtained, but in the opposite direction.

The above results were verified qualitatively by the following experiment. An He-Ne 6328-Å optical beam was coupled into the device which was fabricated in Section III, at various incident directions. In Fig. 10 are the pictures of the output light spot for the incident angle θ_0, θ_1, θ_2, and θ_3, where $\theta_0=0°$ and $\theta_1<\theta_2<\theta_3$. For these pictures, a voltage of 30 V is applied to the device. It is observed that only for $\theta=0°$, the beam is split into two symmetrical positions with the same intensity. For other incident angles, the output light spots are not symmetrical for both position and intensity. A clearer indication on the intensities of output light spots can be seen from Fig. 11, where the intensity profiles of light spots for each incident angle are shown. It is seen that, in general, for $\theta_0<\theta_1<\theta_2<\theta_3$, the deflection angles and intensities vary in a theoretically predicted fashion.

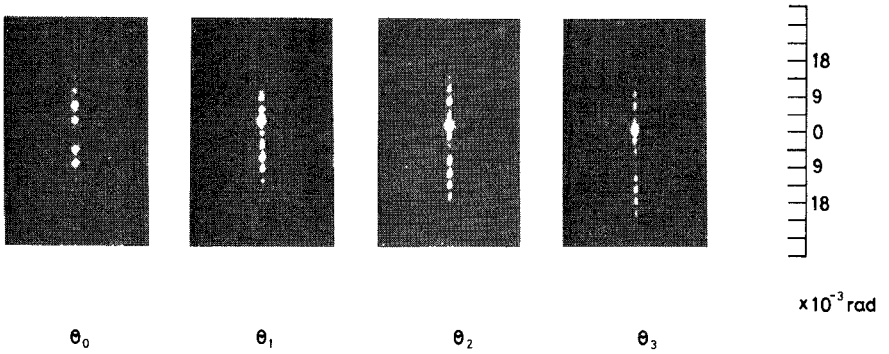

Fig. 10. The output beam spots for the optical beam incident onto the experimental device of Fig. 7 under various incident angles θ_0, θ_1, θ_2, and θ_3, where $\theta_0 = 0°$ and $\theta_0 < \theta_1 < \theta_2 < \theta_3$. The applied voltage was 30 V.

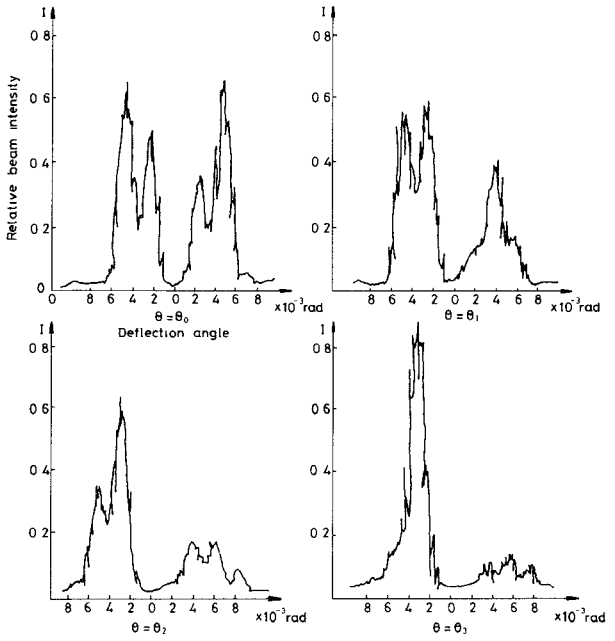

Fig. 11. The intensity profiles of the output beam spots of Fig. 10.

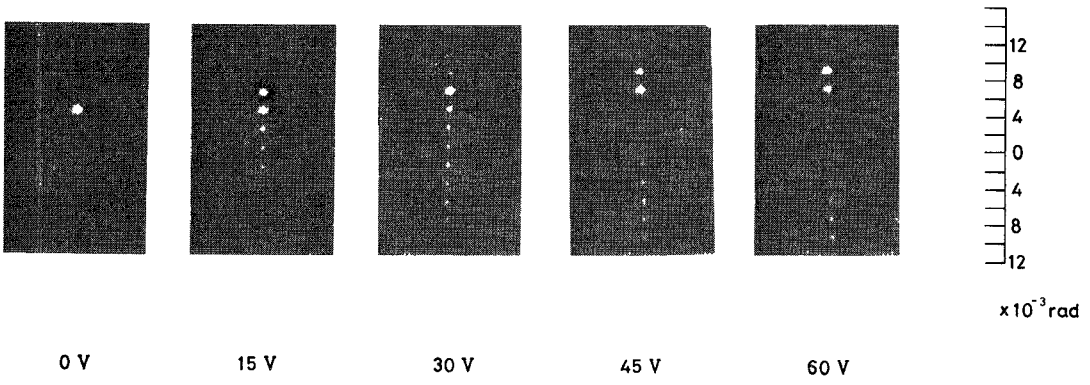

Fig. 12. The output beam spots for the experimental zig-zag array beam splitter of Fig. 7 operating as a beam deflector under various applied voltages.

For $\theta = \theta_d$, the device acts as a pure deflector. Another experiment was done to demonstrate this behavior. The light beam was incident onto the fabricated device with an angle $\theta = \theta_d$. Fig. 12 is the pictures of the output light spots, taken at 110 cm from the device for $V_0 = 0$, 15, 30, 45, and 60 V, respectively. For this case, when the voltage was applied, the light spot shifted to the upper position. As the voltage was increased further, the light spot shifted further away from the central position. This device operated as a voltage-controlled deflector.

In the above experiment, the deflection angle obtained for $V_0 = 30$ V was 4.45×10^{-3} rad, which was just equal to

one half of that of the device when it was operated as a splitter with the same applied voltage. Here we proved again that the deflection angle for a zig-zag electrode is two times greater than that of the conventional prism electrodes.

In addition, in [19], one of the authors (C. L. Lee) proposed an electrode to be a beam splitter and did experimental demonstrations. As the study here reveals, the electrode actually is a beam deflector. The reason that the experimental device demonstrated a beam-splitting characteristics was because the incident angle of the beam was not zero, as explained above.

V. Conclusions

In this paper, we have proposed and studied a new type of electrooptic beam splitter with a zig-zag electrode. Both the theoretical and experimental studies, conducted on a single simulated element, as well as on the array structure, showed that the device behaved as a beam splitter. Due to the simpler electrode configuration, compared to the conventional electrodes, the device is easier to fabricate and is expected to be operable at a higher speed. The device has a deflection power two times greater than the beam splitter with the conventional electrodes. The device can also be used as a beam deflector, if the incident direction of the optical beam is parallel to the direction of electrodes. If the incident optical beam is not normal to the array, but at an angle θ which is smaller than the electrode tilt angle θ_d, the device acts as a combination beam splitter and beam deflector.

Acknowledgment

The technical assistance from Semiconductor Research Center, N.C.T.U., in fabricating experimental devices is appreciated.

References

[1] Yoshiro Ohmachi and Juichi Noda, "Electro-optic light modulator with branched ridge waveguide," *Appl. Phys. Lett.*, vol. 27, pp. 544–546, 1975.

[2] T. R. Ranganath and Shyh Wang, "Ti-diffused $LiNbO_3$ branched-waveguide modulators: performance and design," *IEEE J. Quantum Electron.*, vol. QE-13, pp. 290–295, 1977.

[3] H. Sasaki, "Efficient intensity modulation in a Ti-diffused $LiNbO_3$ branched optical waveguide device," *Electron. Lett.*, vol. 13, no. 23, pp. 693–694, 1977.

[4] Yong-Kyung Lee and Shyh Wang, "Electrooptic Bragg-deflection modulators: Theoretical and experimental studies," *App. Opt.*, vol. 15, no. 6, pp. 1565–1572, 1976.

[5] Masayuki Izutsu, Shinsuke Shikama, and Tadasi Sueta, "Integrated optical SSB modulator/frequency shifter," *IEEE J. Quantum Electron.*, vol. QE-17, pp. 2225–2227, 1981.

[6] Yuichi Ninomiya, "Ultrahigh resolving electrooptic prism array light deflectors," *IEEE J. Quantum Electron.*, vol. QE-9, pp. 791–795, 1973.

[7] I. P. Kaminow and L. W. Stulz, "A planar electrooptic-prism switch," *IEEE J. Quantum Electron.*, QE-11, pp. 633–636, 1975.

[8] C. S. Tsai and P. Saunier, "Ultrafast guided-light beam deflection/switching and modulation using simulated electro-optic prism structures in $LiNbO_3$ waveguides," *Appl. Phys. Lett.*, vol. 27, no. 4, pp. 248–250, 1975.

[9] B. Chen and C. M. Meijer, "Bragg switch for optical channel waveguides," *Appl. Phys. Lett.*, vol. 33, no. 1, pp. 33–35, 1978.

[10] H. Naitoh, K. Muto, and T. Nakayama, "Mirror-type optical branch and switch," *Appl. Opt.*, vol. 17, no. 1, pp. 101–104, 1978.

[11] C. S. Tsai, Bumman Kim, and Fathi R. El-Arrari, "Optical channel waveguide switch and coupler using total internal reflection," *IEEE J. Quantum Electron.*, vol. QE-14, no. 7, pp. 513–517, 1978.

[12] K. Mitsunaga, K. Murakami, M. Masuda, and J. Koyama, "Optical $LiNbO_3$ 3-branched waveguide and its application to a 4-port optical switch," *Appl. Opt.*, vol. 19, no. 22, pp. 3837–3842, 1980.

[13] Hiroshi Terui and Morio Kobayashi, "Total reflection optical waveguide switching through dielectric chip motion," *Appl. Opt.*, vol. 20, no. 18, pp. 3152–3157, 1981.

[14] J. F. Revelli, "High-resolution electrooptic surface prism waveguide deflector: an analysis," *Appl. Opt.*, vol. 19, no. 3, pp. 389–397, 1980.

[15] C. L. Lee and J. Y. Huang, "A double-pole, double throw electro-optic switch with an N-type electrode," *Opt. and Quantum Electron.*, vol. 12, pp. 525–527, 1980.

[16] C. H. Bulmer, W. K. Burns, and T. G. Giallorenzi, "Performance criteria and limitations of electrooptic waveguide array deflectors," *Appl. Opt.*, vol. 18, no. 19, pp. 3282–8295, 1979.

[17] C. L. Lee, J. F. Lee, and J. Y. Huang, "Linear phase shift electrodes for the planar electrooptic prism deflector," *Appl. Opt.*, vol. 19, no. 17, pp. 2902–2905, 1980.

[18] M. Born and E. Wolf, *Principles of Optics*. Edinburgh, Scotland: Pergamon, 1965, pp. 401.

[19] J. Y. Huang and C. L. Lee, "A planar electro-optic prism array beam splitter," *Appl. Phys. Lett.*, vol. 36, no. 7, pp. 507–509, 1980.

Chung Len Lee (S'71–M81') was born in 1946 in Hu-Pei, China. He received the B.S. degree in electrical engineering from the National Taiwan University, Taiwan, Republic of China, in 1968, and the M.S. and Ph.D. degree in electrical engineering from Carnegie-Mellon University, Pittsburgh, PA, in 1971 and 1975, respectively.

In 1975, he joined National Chiao Tung University as a faculty member, engaging in research on various topics on integrated optics, optoelectronics, semiconductor devices, integrated circuits, and process. He has published more than twenty papers in the above areas. Presently, he is a professor and the Director of Semiconductor Research Center of this university.

Mr. Lee is a member of Phi Kappa Phi and Phi Tau Phi.

Jing Shyang Horng was born in Taiwan, Republic of China, in 1958. He received the B.S. degree in electrophysics and the M.S. degree in electro-optical engineering from the National Chiao Tung University, Hsin Chu, Taiwan, Republic of China, in 1980 and 1982, respectively. Presently, he is a Ph.D. student pursuing the Ph.D. degree at this university. His interests include fiber optics, nonlinear optics, and application of laser in microelectronics.

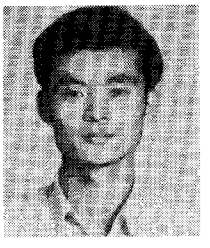

Cheng Hao Huang was born in Taipei, Taiwan, Republic of China, in 1957. He received the B.S. degree from the College of Oceanography, Taiwan, Republic of China, in 1980, and the M.S. degree from the National Chiao Tung University, Taiwan, Republic of China, in 1982. His M.S. thesis work was on the study of integrated optics devices.

Presently, he is working in Chung Shan Institute of Science and Technology, engaging in electronic circuit design.

Mr. Huang is a member of Chinese Optics Engineering Society.